Experimental velocity study of non-Boussinesq Rayleigh-Bénard convection

Valori, Valentina; Elsinga, Gerrit; Rohde, Martin; Tummers, Mark; Westerweel, Jerry; van der Hagen, Tim

DOI
10.1103/PhysRevE.95.053113

Publication date
2017

Document Version
Final published version

Published in
Physical Review E

Experimental velocity study of non-Boussinesq Rayleigh-Bénard convection

Valentina Valori,[1,2,*] Gerrit Elsinga,[2,†] Martin Rohde,[1,‡] Mark Tummers,[2] Jerry Westerweel,[2] and Tim van der Hagen[1]

[1]*Nuclear Energy and Radiation Applications, Faculty of Applied Sciences, Delft University of Technology, Mekelweg 15, 2629JB, Delft, The Netherlands*

[2]*Laboratory for Aero and Hydrodynamics, Faculty of Mechanical, Maritime and Materials Engineering, Delft University of Technology, Mekelweg 2, 2628CD, Delft, The Netherlands*

(Received 27 October 2016; revised manuscript received 4 May 2017; published 25 May 2017)

The effects of strongly varying fluid properties, beyond the validity range of the so-called Boussinesq approximation, were experimentally studied in Rayleigh-Bénard (RB) convection. Two experiments were conducted in the same cubical RB convection cell at similar Rayleigh and Prandtl numbers. In one experiment water was used as working fluid and the imposed temperature difference between the top and bottom plates of the cell was such to ensure non-Boussinesq conditions. In the other experiment, taken as a reference for Boussinesq conditions, methanol was used as working fluid, allowing a smaller temperature difference between the plates. In both experiments the instantaneous and time-averaged flow fields were determined experimentally in a vertical cross section of the cell by using particle image velocimetry. Results show a non-Boussinesq effect that manifests itself as an increase of the time-averaged horizontal velocity component close to the bottom wall of the cell and as a global top-bottom asymmetry of the velocity field. This is an experimental study of the whole velocity field of RB convection at non-Boussinesq conditions.

DOI: 10.1103/PhysRevE.95.053113

I. INTRODUCTION

In the Boussinesq approximation [1], the fluid properties are assumed to be constant in all the terms of the Navier-Stokes equations, except in the buoyancy term. The Boussinesq approximation can be used in many cases to simplify complex problems without a significant loss of accuracy, but there are also many physical phenomena that cannot be understood without considering the temperature dependency of the fluid properties (see, e.g., [2]). In the present paper Rayleigh-Bénard (RB) convection was studied at conditions beyond the Boussinesq approximation, in which the volumetric thermal expansion coefficient, the kinematic viscosity, and the Prandtl number vary significantly with temperature over the flow domain.

There are several earlier studies in literature that focus on RB convection at non-Boussinesq (NB) conditions. In Ahlers *et al.* [3] an experimental and theoretical study on the effects of NB conditions on the Nusselt and Reynolds number is presented, with heat flux and temperature data. Their Reynolds number measurements are based on thermal plumes transient times calculated from temperature auto- and cross-correlation functions [3]. The working fluid in their study is water at atmospheric pressure, which shows significant changes of the kinematic viscosity and the volumetric thermal expansion coefficient in the range of temperatures considered. They observed significant deviations from the Boussinesq approximation in the ratio between the bottom and top thermal boundary layer thicknesses, up to 20% for the studied conditions. However, despite this reduction in the thickness of the bottom boundary layer with respect to the top one, they did not find significant changes of Nusselt and Reynolds numbers due to the temperature dependency of the fluid properties, up to 2%. For similar conditions, Sugiyama *et al.* [4] performed a two-dimensional (2D) direct numerical simulation study with the purpose of analyzing the flow organization of Rayleigh-Bénard convection with variable properties. In this study, no significant differences between the flow structure at NB and at Boussinesq conditions were observed, except for the secondary flow, where an apparent asymmetry emerges between the two small rolls at two opposite corners of the cell. NB effects in the velocity fields of RB convection were also studied in three-dimensional (3D) numerical simulations in glycerol and water by Horn *et al.* [5,6]. In these studies differences due to NB effects were observed in the mean velocity profiles as bottom-top asymmetries of the horizontal velocity component and in the thickness of the bottom kinetic boundary layer. More specifically, they found an increase of the horizontal component of the velocity and a decrease of the kinetic boundary layer close to the bottom wall of the cell. Both aspects were attributed to non-Boussinesq effects due to the temperature dependency of the kinematic viscosity. NB conditions in glycerol were experimentally studied with velocity measurements in the thermal sublayers through temperature fluctuation signals by Zhang *et al.* [7]. They observed that the second derivative of the velocity profile has a different sign in the thermal sublayer close to the bottom wall of the cell (positive sign) with respect to the top thermal sublayer (negative sign). The change in the second derivative of the velocity in the thermal sublayers was explained as a response of the velocity to the kinematic viscosity changes (due to a strong temperature dependency of the kinematic viscosity) and the maintenance of a constant viscous stress in a steady thermal layer. There are no experimental studies in the literature of the whole velocity field of RB convection under NB conditions.

The objective of the present study is to experimentally determine the effects of NB conditions on the whole velocity field in a vertical cross section of RB convection. This is an

*v.valori@tudelft.nl
†g.e.elsinga@tudelft.nl
‡m.rohde@tudelft.nl

experimental verification on a 3D domain and with accurate direct velocity measurements of the several numerical and theoretical [3–6] studies on NB effects in the velocity fields of RB convection.

In this study the characteristics of measured velocity fields under NB conditions in a 77-mm-high cubical RB convection cell were compared with the velocity fields of a control experiment done in the same setup at Boussinesq conditions. NB conditions were created with a temperature difference of 40 K imposed on the cell while it was filled with water. This resulted in $\mathrm{Ra} = 6.9 \times 10^8$ and $\mathrm{Pr} = 4.3$. The reference case for Boussinesq conditions considered a 9.6 K temperature difference between the bottom and top plates of the cell, resulting in a Rayleigh number of 6.7×10^8 and a Prandtl number of 7.2, with methanol as working fluid. Methanol was chosen to maintain similar Rayleigh and Prandtl numbers in the Boussinesq case with respect to the NB one, while using the same setup for both experiments. Particle image velocimetry was then applied to determine the mean velocities and the rms values of the velocity fluctuations in a vertical cross section of the RB convection cell for both the Boussinesq and the NB case. From the experimental velocity fields a NB effect emerges as top-bottom asymmetries in the mean velocity of the flow.

II. EXPERIMENTAL SETUP

The Rayleigh-Bénard cell used for the experiments is a cube of 77 mm inner length (H) (see Fig. 1). It has four 1.2-mm-thick vertical glass walls that allow for optical access and two horizontal copper plates. The bottom copper wall is electrically heated by a heating strip with adjustable power. The top copper wall is water cooled. The temperature of the cooling water can be regulated to maintain the temperature of the top plate to the desired value. Four thermistors are located in each one of the horizontal walls to monitor the uniformity of the temperature in the plates. The thermistors are made of

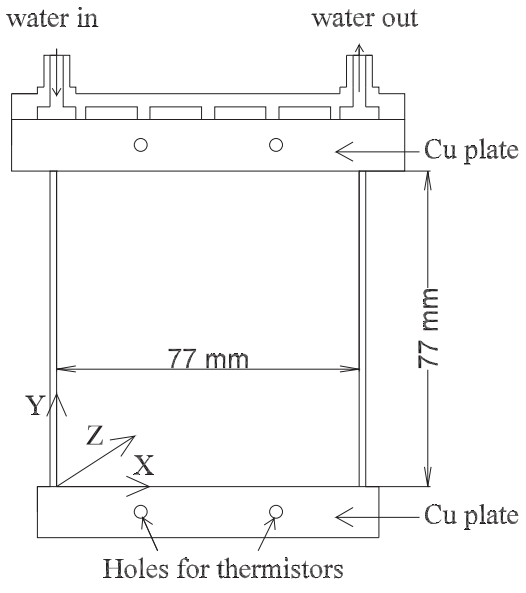

FIG. 1. Sketch of a vertical section of the Rayleigh-Bénard cell.

TABLE I. Upper bounds for the statistical relative uncertainties of the measured quantities.

Quantity	T	$\overline{u_X}, \overline{u_Y}$	$\mathrm{rms}(u'_X, u'_Y)$
Rel. unc. NB	1%	3%	11%
Rel. unc. Boussinesq	1%	7%	13%

epoxy coated negative temperature coefficient (NTC) of type C100. The cell is slightly tilted, less than 3° on the horizontal plane (XZ plane) in diagonal direction, in order to fix the orientation of the large-scale circulation (LSC). Further details about the apparatus can be found in [8].

A. Particle image velocimetry equipment and measurement uncertainty

Planar particle image velocimetry (PIV) measurements were performed in a vertical cross section of the convection cell, at half the depth of the domain ($Z/H = 0.5$). A diode laser (Pegasus) with a power of 400 mW and a wavelength of 520 nm was used to create a light sheet for the illumination of seeding particles in the measurement section. Two kinds of particles were chosen for the experiments with water and methanol. In water, fluorescent particles were used with the purpose of avoiding the effect of reflections off the glass walls of the laser light in the images and improving the quality of the measurements close to the wall. The fluorescent particles (Fluostar) have an average diameter of 13 μm and a density of 1.1 g/cm^3. The fluorescent dye is rhodamine B, which is excited by a wavelength of 550 nm and emits at 580 nm. A long pass optical filter was placed in front of the camera to block the laser light and visualize only the fluorescent emission of the particles. For the experiments with methanol it was not possible to use fluorescent seeding for reasons of chemical incompatibility of the particles with alcohols. Silver coated particles (Dantec) were used in methanol instead. These particles have an average diameter of 10 μm and a density of 1.4 g/cm^3. A PIV camera (LaVision Imager Intense) with a resolution of 1088×1040 pixels was used for the recordings. In the experiments done with silver coated particles a background image subtraction was applied to the camera recordings, with the aim of reducing the effect of reflections of the laser light in the images off the glass walls.

The camera was equipped with an objective with a focal length of 60 mm and aperture stop $f_\# = 8$. The magnification factor of the recordings is $M = 0.055$. Velocities are measured with a second pass interrogation window of 16×16 pixels and an overlap of 50%, which corresponds to a resolution in space of 0.65 mm (8 pixels or 0.008 times the height of the cell). The laser was triggered with a pulse separation time of 0.030 s, corresponding to a particle image displacement between frames of about 6 pixels in the highest velocity regions of the NB experiment. For each experiment 10 800 frames were acquired during 1-h-long measurements, which corresponds to more than 100 turnover times of the LSC motion. To ensure steady state of the flow, the measurements were done after running the setup at constant conditions for about 4 h. To double-check the steady state of the flow, the experiments were repeated twice on different days with results

TABLE II. Experimental conditions and comparison between the relative changes of α, ν, and Pr from the bottom to the top of the cell. All the properties in the nondimensional numbers are taken at the average temperature between the bottom and top wall temperatures of the cell (indicated as T_m). The values of the properties of both water and methanol were taken from REFPROP version 9.1 [9].

Expt. conditions	Fluid	Ra	Pr	T_m	ΔT	$\frac{\Delta\alpha}{\alpha_{\text{top}}}$	$\frac{\Delta\nu}{\nu_{\text{top}}}$	$\frac{\Delta\text{Pr}}{\text{Pr}_{\text{top}}}$
Non-Boussinesq	Water	6.91×10^8	4.33	40 °C	40°C	153%	−52%	−57%
Boussinesq	Methanol	6.74×10^8	7.24	20 °C	9.6 °C	1.5%	−13%	−11%

that confirm the previous ones. They are shown in Figures 4, 5, 7, 8, and 9. In Figures 4, 5, 8 and 9, two versions of each case are plotted as one-line profiles. The repeated experiments are called non-Boussinesq 2nd and Boussinesq 2nd. Figure 7 shows the contour plots of only the second experiment of each case (non-Boussinesq 2nd and Boussinesq 2nd), while the first experiment is in Fig. 6. Small differences between the first experiments and the repeated ones are mainly due to statistical uncertainty of the velocity measurements.

For each component of the velocity field, the mean velocity magnitude and the rms of the fluctuating velocity component, defined by the Reynolds decomposition $u_i = \overline{u_i} + u_i'$, were computed from PIV measurements as described in (1)–(3):

$$\overline{u_i} = \frac{\sum_{j=1}^{N} u_{i,j}}{N}, \tag{1}$$

$$\overline{u_i' u_i'} = \overline{u_i^2} - \overline{u_i}^2, \tag{2}$$

$$\text{rms}(u_i') = \sqrt{\overline{u_i' u_i'}}, \tag{3}$$

where $i = X, Y$ and N is the number of frames. The turbulent kinetic energy (k) is defined on the basis of the rms of the velocity fluctuations as

$$k = \frac{1}{2} \sum_{i=X,Y} \overline{u_i' u_i'}. \tag{4}$$

The statistical uncertainty of the mean velocity values of the NB and the Boussinesq case was respectively estimated as 3% and 7% of their measured values and the statistical uncertainty of the rms of the fluctuating velocity values was estimated as 11% and 13% of their measured values, respectively. They were computed from (5) and (6), where n is the number of independent samples, estimated as in (7). Since Eqs. (5) and (6) refer to a single measurement point, the values of for the relative uncertainties of the mean and rms velocity values are taken in the point where they assume their highest value and rounded to the highest integer.

$$\text{Rel. unc.}(u_i) = \frac{\sqrt{\overline{u_i' u_i'}}}{\overline{u_i}\sqrt{n}}, \tag{5}$$

$$\text{Rel. unc.}(\sqrt{\overline{u_i' u_i'}}) = \sqrt{\frac{2}{n}}, \tag{6}$$

$$n = \frac{N}{\frac{4 \times H}{0.9 \times \overline{u}_{\max}} f}, \tag{7}$$

where the frequency f is three frames/s. In Table I values for the upper bounds of the relative uncertainties of the measured quantities are reported.

TABLE III. Measured LSC ($U_{\text{LSC expt.}}$) and LSC estimated with the Gossmann-Lohse theory ($U_{\text{LSC(GL)}}$) and the model from Pandey *et al.* [13,14] ($U_{\text{LSC}(P)}$). The measured LSC velocity represents the maximum of the time-average vertical velocity.

Expt. conditions	$U_{\text{LSC expt.}}$[m/s]	$U_{\text{LSC(GL)}}$[m/s]	$U_{\text{LSC}(P)}$[m/s]
Non-Boussinesq	16.4×10^{-3}	9.5×10^{-3}	15.3×10^{-3}
Boussinesq	12×10^{-3}	7.5×10^{-3}	12.9×10^{-3}

III. EXPERIMENTAL PROCEDURE AND VELOCITY SCALING

Two different experimental conditions were studied (see Table II), which have been called the NB and the Boussinesq case. At NB conditions the temperature difference between the bottom and the top plates of the cell leads to fluid property differences that are beyond the Boussinesq approximation, while in the Boussinesq case the temperature difference applied to the two horizontal plates of the cell results in smaller changes of fluid properties. The Boussinesq experiment was done in the same experimental setup of the non-NB experiment to show that the NB effects seen in the NB case are due to the strong temperature dependency of the fluid properties and not to the experimental apparatus used for the measurements.

The two experiments were done at similar Rayleigh and Prandtl numbers. The Rayleigh and Prandtl numbers are the two nondimensional parameters that govern the flow for a given geometry of the domain. They are obtained after nondimensionalization of the Navier-Stokes equations, under Boussinesq conditions. The Rayleigh number is defined as

$$\text{Ra} \equiv \frac{\alpha_m g \Delta T H^3}{\nu_m \kappa_m}, \tag{8}$$

where α is the volumetric thermal expansion coefficient of the fluid, g the gravitational acceleration, ΔT the difference of temperature between the hot bottom plate and the cold top plate of the cell, H the distance between the two horizontal plates, ν the kinematic viscosity of the fluid, and κ the thermal diffusivity of the fluid. The Prandtl number is defined as the ratio between kinematic viscosity and thermal diffusivity:

$$\text{Pr} \equiv \frac{\nu_m}{\kappa_m}. \tag{9}$$

All the fluid properties used in the calculation of the nondimensional numbers are taken at the average temperature between the bottom and the top wall temperature of the cell,

T_m, reported in Table II . This is indicated with a subscript m in the symbol of the fluid property.

To maintain the same Rayleigh number in the same setup, both for the Boussinesq and the non-Boussinesq case, the experiment at Boussinesq conditions was done with methanol, while the working fluid in the NB case was water.

In Table II are given the experimental conditions of the two cases, together with an example of the changes of the values of two fluid properties and of the Prandtl number between the bottom and the top plates of the cell. The two properties considered are the volumetric thermal expansion coefficient (α) and the kinematic viscosity (ν), because these are the properties of water that show the largest change at atmospheric pressure. In the last column, also the change on Prandtl number throughout the cell due to its temperature dependency is given for both fluids.

To make the flow fields dimensionless, taking into account the influence of the variation in Pr number between the two experiments (Pr = 4.33 in the NB case and Pr = 7.24 in the Boussinesq one), the velocity values were scaled by a characteristic LSC velocity of the flow. Currently in literature there are two possible ways to determine the LSC velocity of the flow as a function of the Rayleigh and Prandtl number with the Boussineq approximation: the Grossmann-Lohse theory [10–12] and the scaling method proposed by Pandey *et al.* [13,14].

The Grossmann-Lohse theory, summarized by Ahlers *et al.* [15] allows for the prediction of a typical Reynolds number and Nusselt number as a function of the Rayleigh number and Prandtl number, for cells of aspect-ratio-one at Boussinesq conditions. The LSC velocity used for the scaling is calculated from the Reynolds number predicted by the GL theory as

$$U_{\mathrm{LSC\ (GL)}} = \mathrm{Re}\frac{\nu_m}{H}. \tag{10}$$

The equations of the Gossmann-Lohse (GL) theory that were used for the velocity scaling are

$$(\mathrm{Nu}-1)\mathrm{Ra}\,\mathrm{Pr}^{-2} = c_{1(\mathrm{GL})}\frac{\mathrm{Re}^2}{g(\sqrt{\mathrm{Re}_L/\mathrm{Re}})} + c_{2(\mathrm{GL})}\mathrm{Re}^3, \tag{11}$$

$$\mathrm{Nu}-1 = c_{3(\mathrm{GL})}\mathrm{Re}^{1/2}\mathrm{Pr}^{1/2}\left\{f\left[\frac{2a\,\mathrm{Nu}}{\sqrt{\mathrm{Re}_L}}g\left(\sqrt{\frac{\mathrm{Re}_L}{\mathrm{Re}}}\right)\right]\right\} + c_{4(\mathrm{GL})}\mathrm{Pr}\,\mathrm{Re}\,f\left[\frac{2a\,\mathrm{Nu}}{\sqrt{\mathrm{Re}_c}}g\left(\sqrt{\frac{\mathrm{Re}_L}{\mathrm{Re}}}\right)\right]. \tag{12}$$

The following constants and formulas were applied [16]:

$$c_{1(\mathrm{GL})} = 8.05,\ c_{2(\mathrm{GL})} = 1.38,\ c_{3(\mathrm{GL})} = 0.487,$$
$$c_{4(\mathrm{GL})} = 0.0252,\ a = 0.922,\ \mathrm{Re}_L = (2a)^2, \tag{13}$$

$$f(x_\theta) = \left(1+x_\theta^4\right)^{-1/4}, \qquad x_\theta = 2a\frac{\mathrm{Nu}}{\sqrt{\mathrm{Re}}}, \tag{14}$$

$$g(x_L) = x_L\left(1+x_L^4\right)^{-1/4}, \qquad x_L = \sqrt{\frac{\mathrm{Re}_L}{\mathrm{Re}}}. \tag{15}$$

Both Ra and Pr are known (from the experiments). Hence by solving Eqs. (11) and (12) the Re number can be computed and from Eq. (10) the velocity scale $U_{\mathrm{LSC(GL)}}$ can be determined.

The method proposed by Pandey *et al.* [13,14] is a different way, with respect to the GL theory, to calculate the LSC velocity of the flow on the base of the Rayleigh and Prandtl numbers, under Boussinesq conditions. It is valid for arbitrary Rayleigh and Prandtl numbers. It is based on the comparison among the relative strength of the nonlinear pressure, buoyancy, and viscous terms of the momentum equation of RB convection. In the turbulent regime, which is characterized by Ra $\gg 10^6$ Pr, the LSC velocity can be

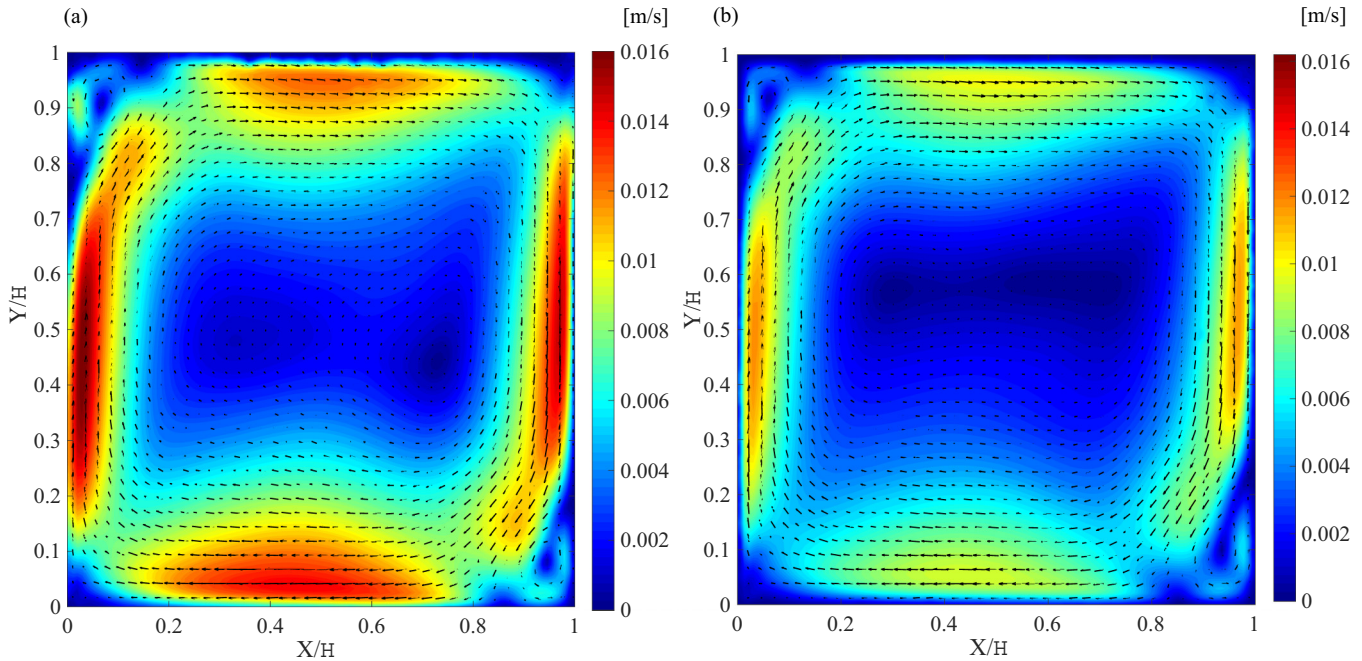

FIG. 2. Mean velocities ($|\overline{u}|$) contour plots in a vertical cross section at half-depth of the cell ($Z/H = 0.5$). (a) Non-Boussinesq: Ra = 6.91×10^8, Pr = 4.33; (b) Boussinesq: Ra = 6.74×10^8, Pr = 7.24.

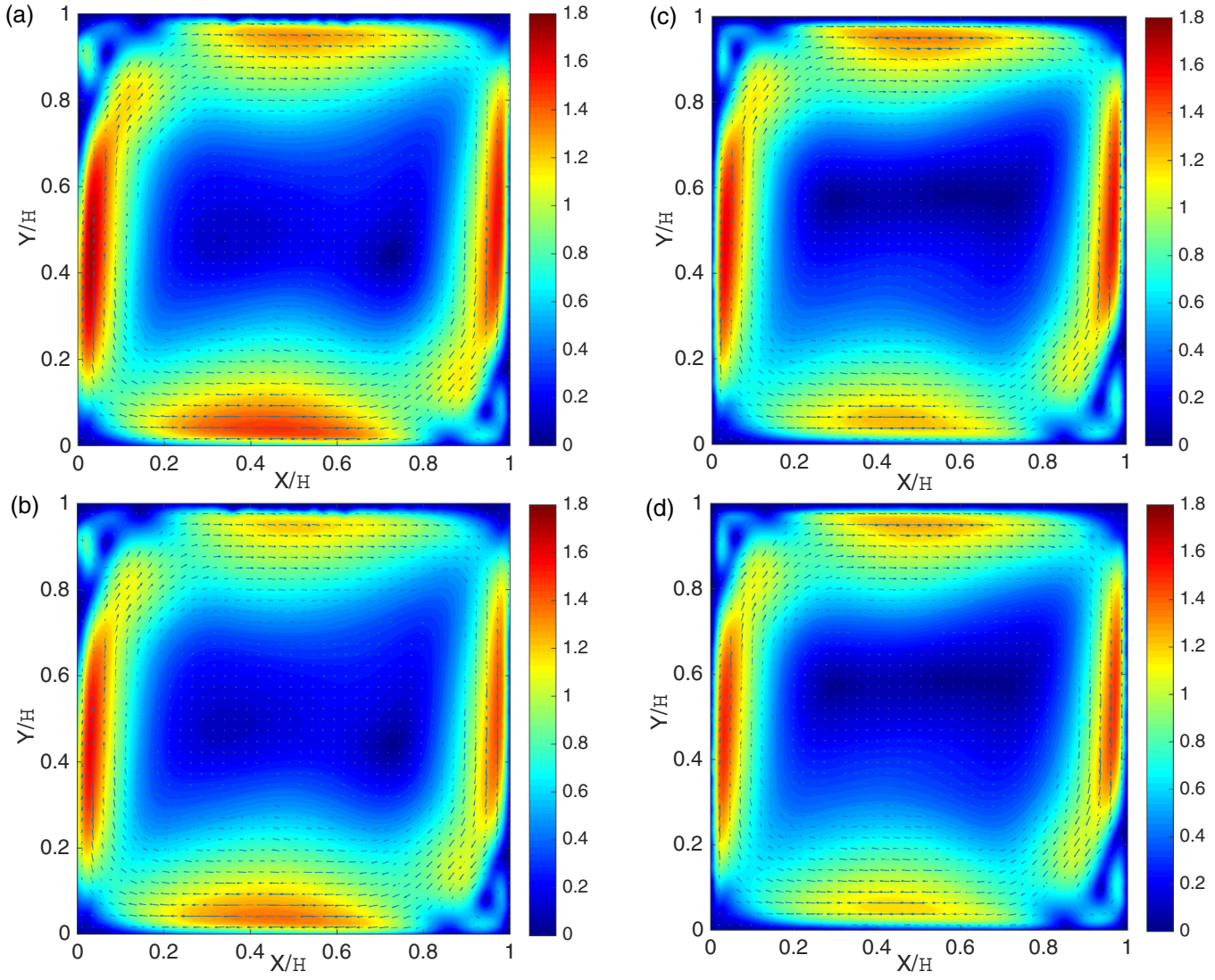

FIG. 3. Mean velocities ($|\overline{u}|$) contour plots in a vertical cross section at half-depth of the cell ($Z/H = 0.5$). Velocity values normalized by $U_{\mathrm{LSC(GL)}}$ in panels (a) and (c) and by $U_{\mathrm{LSC}(P)}$ in panels (b) and (d). Panels (a) and (b) Non-Boussinesq: $\mathrm{Ra} = 6.91 \times 10^8$, $\mathrm{Pr} = 4.33$; panels (c) and (d) Boussinesq: $\mathrm{Ra} = 6.74 \times 10^8$, $\mathrm{Pr} = 7.24$.

computed with the formulas (16)–(20) [14]:

$$U_{\mathrm{LSC}(P)} = \mathrm{Pe}\frac{H}{\kappa_m} \tag{16}$$

where κ is the thermal diffusivity of the fluid, taken at the average temperature between the bottom and top wall temperatures of the cell, T_m, and Pe is the Péclet number computed from (17):

$$\mathrm{Pe} = \sqrt{\frac{c_{3(P)}}{|c_{1(P)} - c_{2(P)}|}}, \tag{17}$$

$$c_{1(P)} = 1.5\ \mathrm{Ra}^{0.10}\mathrm{Pr}^{-0.06}, \tag{18}$$

$$c_{2(P)} = 1.6\ \mathrm{Ra}^{0.09}\mathrm{Pr}^{-0.08}, \tag{19}$$

$$c_{3(P)} = 0.75\ \mathrm{Ra}^{-0.15}\mathrm{Pr}^{-0.05}. \tag{20}$$

As summarized in the paper about scaling of large-scale quantities in RB convection by Pandey *et al.* [13], there are several possible ways to calculate the U_{LSC} of the flow. U_{LSC} can be quantified, for example, as the maximum absolute value of the horizontal or of the vertical mean velocity component, or on the basis of their rms's. In the present study U_{LSC} was computed from the experimental data as the absolute value of the maximum of the mean vertical velocity component, because it is less affected by NB effects with respect to the horizontal velocity component or to the velocity rms values. The LSC velocity computed from the experimental data as the peak of the time-average vertical velocity profile together with the LSC velocities estimated from the GL theory and from the formula of Pandey *et al.* [14], are all reported in Table III.

From the comparison among the experimental U_{LSC} and the two LSC scaling velocities that were theoretically predicted on the basis of the Rayleigh and Prandtl numbers of the experiments (see Table III), several interesting observations can be made.

One is that the model proposed by Pandey *et al.* [13,14] matches the experimental values very well for both the

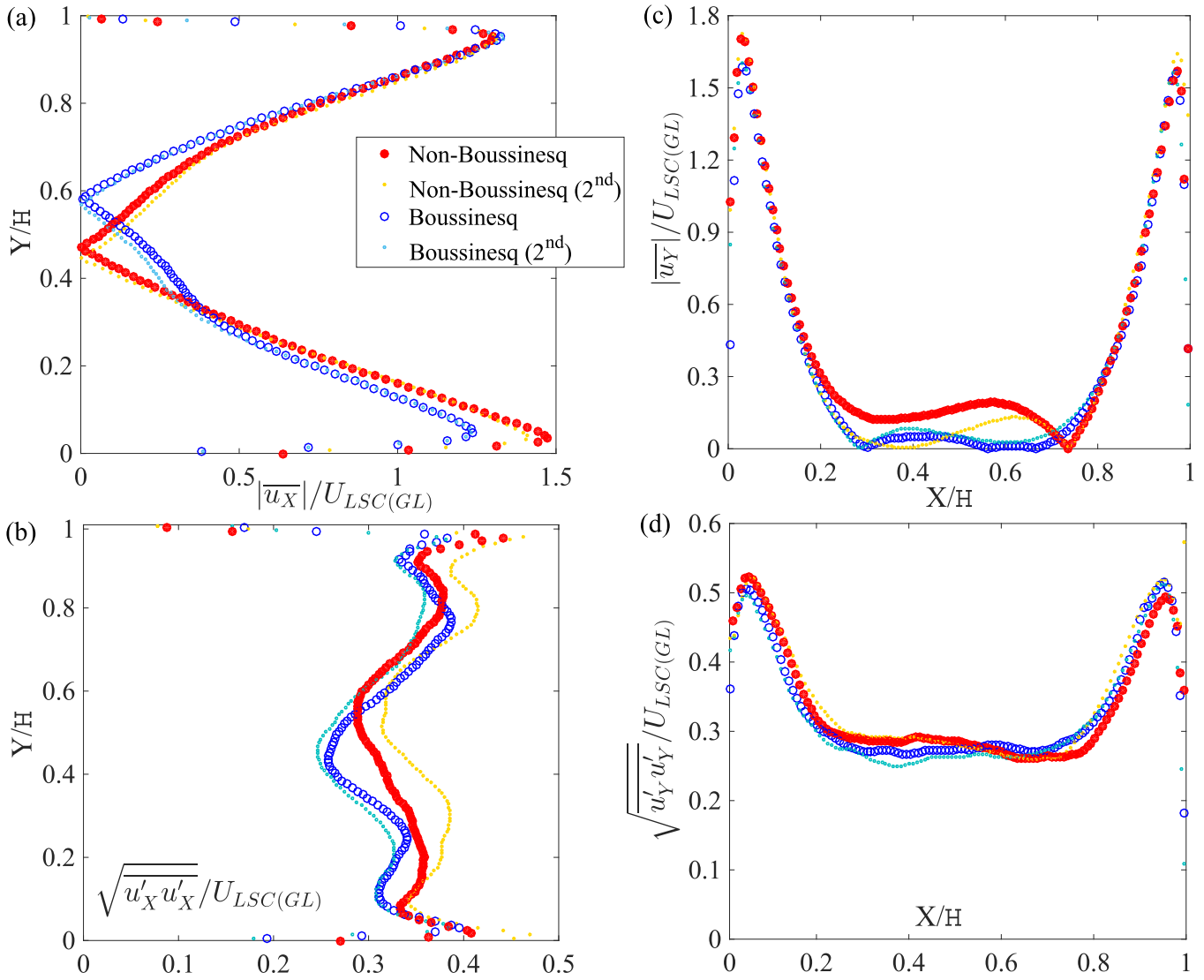

FIG. 4. Comparison between non-Boussinesq and Boussinesq mean velocity [panels (a) and (c)] and velocity fluctuations rms [panels (b) and (d)] at half-depth of the cell ($Z/H = 0.5$). Velocity values normalized by $U_{\mathrm{LSC(GL)}}$. Panels (a) and (b): horizontal component along the line $X/H = 0.5$. Panels (c) and (d): vertical component along the line $Y/H = 0.5$. Non-Boussinesq: Ra $= 6.91 \times 10^8$, Pr $= 4.33$; non-Boussinesq 2nd: Ra $= 6.84 \times 10^8$, Pr $= 4.33$; Boussinesq: Ra $= 6.74 \times 10^8$, Pr $= 7.24$; Boussinesq 2nd: Ra $= 6.77 \times 10^8$, Pr $= 7.24$.

Boussinesq and the NB case. The relative difference between the predicted velocity and the experimental one is indeed within 7.5% for both cases. The relative difference of the U_{LSC} predicted with the GL theory with respect to the experimental values is instead quite large for both the NB and the Boussinesq case; 73% and 60%, respectively. From Table III it can also be seen that while the GL theory underestimates both the NB case and the Boussinesq case, the Pandey model underestimated the NB case and overestimates the Boussinesq case. Eventually another interesting observation that can be made from Table III is that the ratio between the measured U_{LSC} for the NB case and the Boussinesq case ($16.4/12 = 1.37$) is matched better by the predictions of the GL theory ($9.5/7.5 = 1.27$) than by the Pandey model ($15.3/12.9 = 1.19$). The data presented in this paper were scaled both by $U_{\mathrm{LSC(GL)}}$ and by $U_{\mathrm{LSC}(P)}$, in order to show that the choice of one scaling velocity with respect to the other one does not make any difference with regard to the NB effects found. The NB effects indeed were presented as top-bottom asymmetries within one experiment and the Boussinesq experiment was used as a reference case done in the same setup to show that the NB effects seen in the NB case are independent of the experimental apparatus.

IV. RESULTS

A. Mean velocities

The mean velocity field in a vertical cross section at half-depth of the cell ($Z/H = 0.5$) is shown in Fig. 2 . The NB case is presented in panel (a), while the Boussinesq case is presented in panel (b). It can be seen that the velocity fields show a similar shape in both cases: a large roll in the center (the large-scale circulation of the flow) and two small counter-rotating rolls in the upper-left corner and in the bottom-right corner. This agrees with what was reported by Xia *et al.* [17] at a similar Rayleigh number under Boussinesq conditions. In particular,

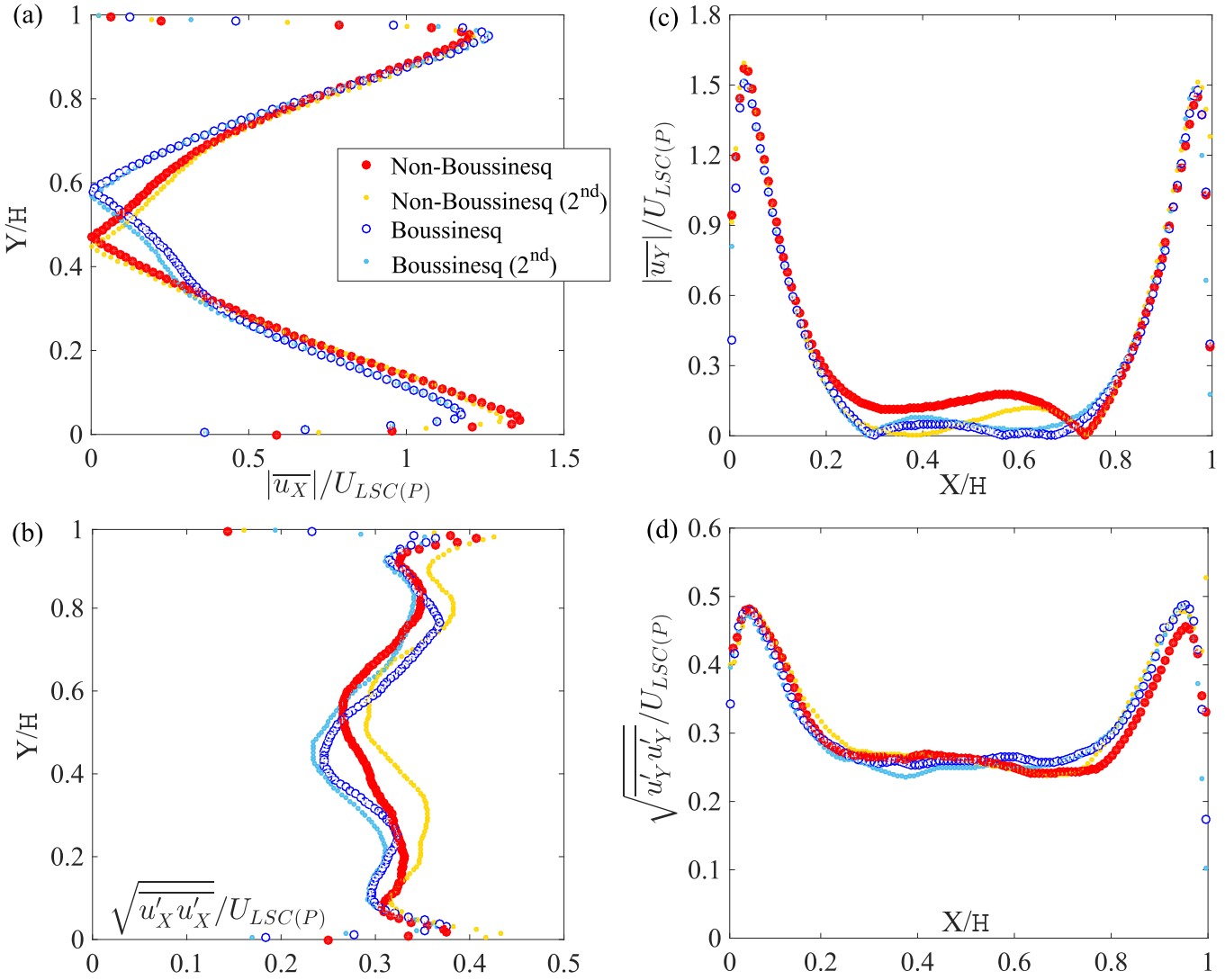

FIG. 5. Comparison between non-Boussinesq and Boussinesq mean velocity [panels (a) and (c)] and velocity fluctuations rms [panels (b) and (d)] at half-depth of the cell ($Z/H = 0.5$). Velocity values normalized by $U_{\mathrm{LSC}(P)}$. Panels (a) and (b): horizontal component along the line $X/H = 0.5$. Panels (c) and (d): vertical component along the line $Y/H = 0.5$. Non-Boussinesq: Ra $= 6.91 \times 10^8$, Pr $= 4.33$; non-Boussinesq 2nd: Ra $= 6.84 \times 10^8$, Pr $= 4.33$; Boussinesq: Ra $= 6.74 \times 10^8$, Pr $= 7.24$; Boussinesq 2nd: Ra $= 6.77 \times 10^8$, Pr $= 7.24$.

the presence of the two corner rolls in the velocity field was found in previous literature as an expression of a characteristic velocity mode of the studied Rayleigh and Prandtl numbers. This mode was identified as responsible for flow reversals [18–20]. It is also interesting to observe that corner rolls were also found in 2D numerical simulations done at similar Rayleigh and Prandtl numbers of our NB experiment, at NB conditions in water by Sugiyama *et al.* [4]. By looking at the corner rolls of Sugiyama *et al.* [4], it can be seen that they are characterized by a spatial extension of about 0.4 X/H, while the spatial extension of the rolls in our 3D experiment is about 0.15 X/H. This consideration, however, cannot be considered a direct comparison between the simulations of Sugiyama *et al.* and our study, because of the difference between 2D simulations and experiments in a 3D geometry and because of similar but not perfectly matching Rayleigh numbers in the two studies (Ra $= 10^8$ in the simulations; Ra $= 6.91 \times 10^8$ in the experiment).

By comparing the NB case and the Boussinesq case shown in Fig. 2, one can observe that the magnitude of the velocity values is higher for the NB case than for the Boussinesq case. The same plots, scaled by $U_{\mathrm{LSC(GL)}}$ and $U_{\mathrm{LSC}(P)}$ are shown in Fig. 3, panels (a),(c) and (b),(d), respectively. After scaling, the magnitude of the velocity fields is similar in the two cases as can be seen by comparing panels (a) and (c) of Fig. 3, and panels (b) and (d) of the same figure. The differences before scaling are mainly due to the different Prandtl numbers. In particular, the NB case is the one with the smaller Prandtl number, and consequently the larger magnitude of the velocity field. The velocity scaling allowed us to normalize the velocities by taking into account the influence of the Prandtl number on the LSC velocity. The two small rolls cannot be scaled by the same scaling velocity that was used for the center roll, indicating that more than one characteristic velocity scale is present in the flow. Hence, the relative importance of a characteristic velocity scale of the

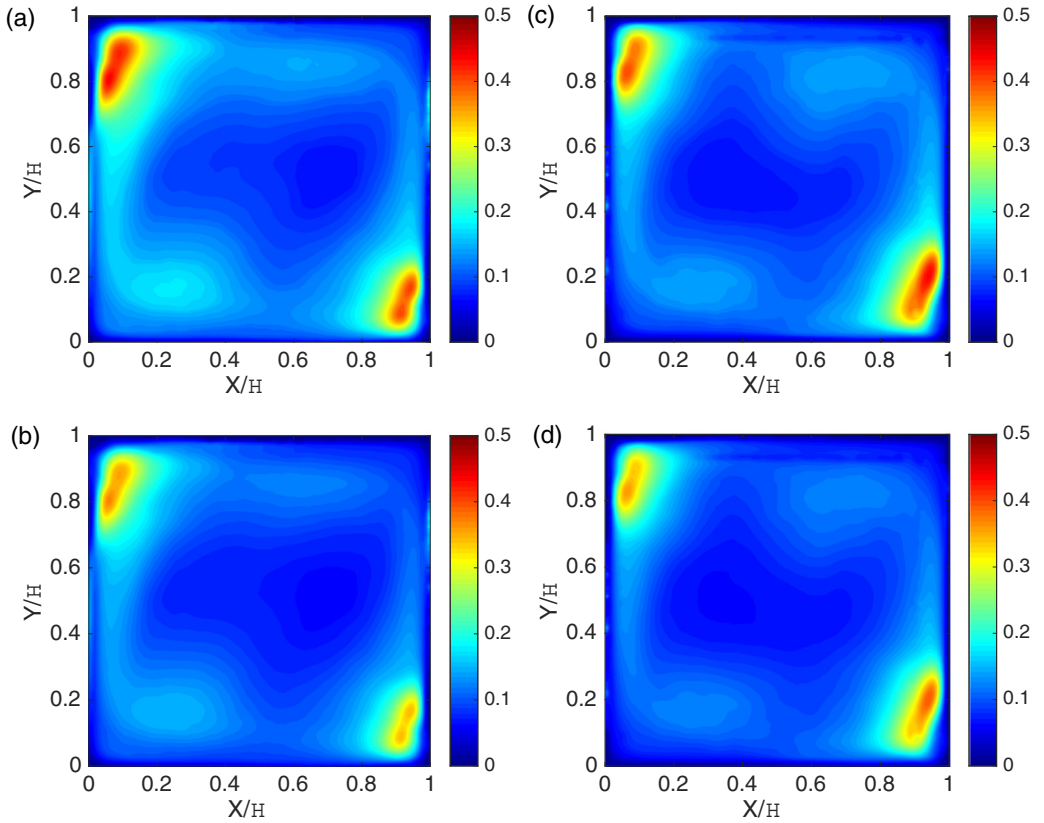

FIG. 6. Turbulent kinetic energy in a vertical cross section at half-depth of the cell ($Z/H = 0.5$). Values normalized by $U_{\mathrm{LSC(GL)}}$ in panels (a) and (c) and by $U_{\mathrm{LSC}(P)}$ in panels (b) and (d). Panels (a) and (b): Non-Boussinesq: Ra $= 6.91 \times 10^8$, Pr $= 4.33$. Panels (c) and (d): Boussinesq: Ra $= 6.74 \times 10^8$, Pr $= 7.24$.

secondary flow with respect to the LSC velocity scale may change, depending on how large the temperature dependency deviates from Boussinesq conditions.

For a more quantitative comparison of the two cases, the values of the horizontal and vertical velocity components along the lines $X/H = 0.5$ and at $Y/H = 0.5$ are shown in Figs. 4 and 5, scaled by $U_{\mathrm{LSC(GL)}}$ and $U_{\mathrm{LSC}(P)}$, respectively. From Fig. 4 (and Fig. 5), panel (a), it can be seen that in the NB case the peak of the horizontal velocity component close to the bottom wall is significantly larger than close to the top wall. The difference is about 13.4%, which is larger than the statistical uncertainty of 3% and 7% of the NB case and the Boussinesq case, respectively. Also, the slope of the boundary layer at the bottom wall is steeper than at the top for the NB case. The increase of the velocity close to the bottom wall of the cell with respect to the region close to the top wall can be explained by the lower values of the kinematic viscosity close to the hot bottom wall of the cell. These findings are consistent with the NB effects observed in 3D numerical simulations by Horn *et al.* [5,6]. Indeed they also note an increase of the horizontal velocity magnitude and a reduction of the kinetic boundary layer thickness near the bottom wall of the cell, with respect to the top wall, due to the temperature dependency of the kinematic viscosity. To show that the NB effects seen in the experiment are due to the temperature dependency of the fluid properties and that they do not depend on the particular apparatus used for the measurements, a Boussinesq case (see Table II) was done in the same setup and used for comparison in the plots. This case, being more Boussinesq than the NB case studied, is characterized by more symmetric top-bottom profiles, with a slight asymmetry of the top-bottom velocity peaks just above the uncertainty limit of 7% (see Figs. 4 and 5).

From Fig. 4 (and Fig. 5), panel (a), one can also observe that the horizontal velocity component plotted along the line $X/H = 0.5$ shows two linear parts in the central region of the cell, at $0.1 \lesssim Y/H \lesssim 0.3$ and $0.7 \lesssim Y/H \lesssim 0.9$, for both the NB case and the Boussinesq case. This was also observed by Xia *et al.* [17] under Boussinesq conditions at similar Rayleigh number. While the slopes of the horizontal velocity component in Fig. 4 (and Fig. 5), panel (a), for NB and Boussinesq conditions are similar in the top part ($0.7 \lesssim Y/H \lesssim 0.9$), they are different near the bottom ($0.1 \lesssim Y/H \lesssim 0.3$). This is related to the large difference between the horizontal velocity peaks close to the bottom wall compared to the top in the NB case. It is also interesting to observe a further difference between the two cases in the central region of the cell for $0.3 \lesssim Y/H \lesssim 0.7$ where both the NB and the Boussinesq profiles show an inflection point, albeit at different locations. In particular, from Fig. 4 (and Fig. 5), it can be seen that both the mean horizontal [panel (a)] and vertical [panel (c)] velocity component values are different from zero at the center of the cell ($Y/H = 0.5$ or $X/H = 0.5$, respectively) for the NB case of quantities that are larger than the statistical uncertainty. This effect is also present in the Boussinesq values of the

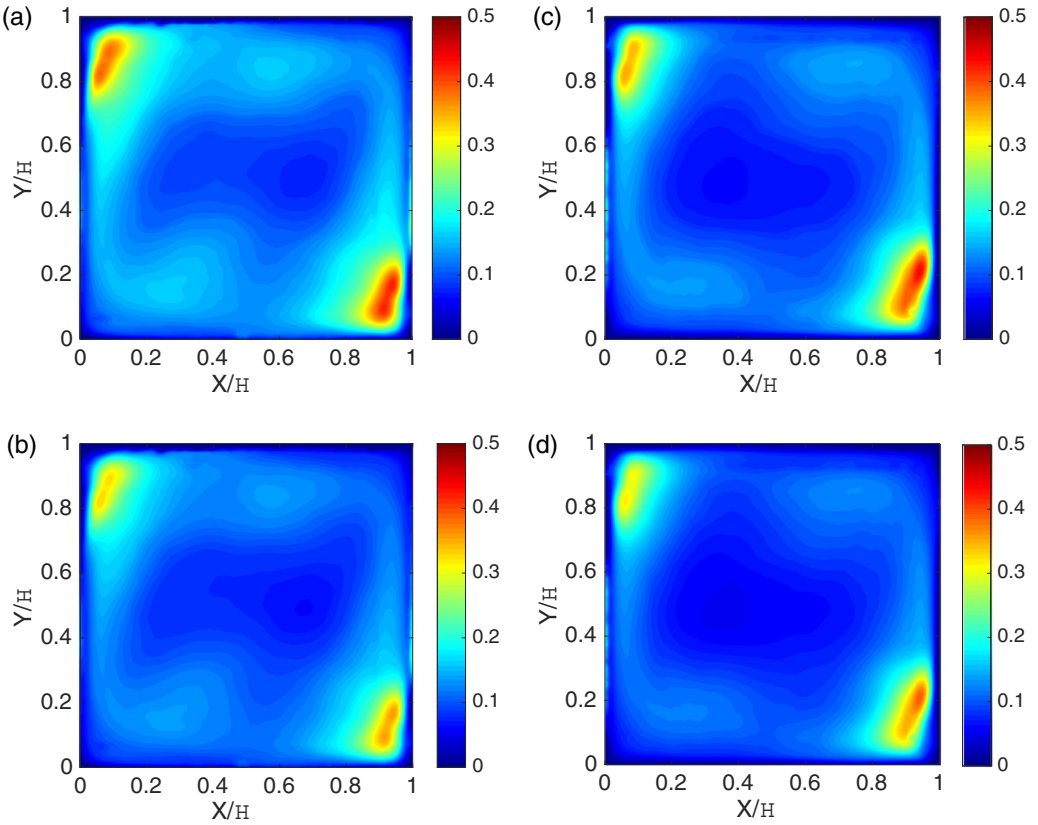

FIG. 7. Turbulent kinetic energy in a vertical cross section at half-depth of the cell ($Z/H = 0.5$) (repeated experiments). Values normalized by $U_{\mathrm{LSC(GL)}}$ in panels (a) and (c) and by $U_{\mathrm{LSC}(P)}$ in panels (b) and (d). Panels (a) and (b): non-Boussinesq 2nd: $\mathrm{Ra} = 6.84 \times 10^8$, $\mathrm{Pr} = 4.33$. Panels (c) and (d): Boussinesq 2nd: $\mathrm{Ra} = 6.77 \times 10^8$, $\mathrm{Pr} = 7.24$.

mean horizontal velocity component [Figs. 4 and 5, panel (a)]. Since for a perfect Boussinesq case, one would expect a zero mean velocity value at the center of the cell, deviations from zero show that the nominal Boussinesq case is also affected by NB effects.

This top-bottom asymmetry NB effect agrees with previous numerical studies [5,6] (Fig. 9) and confirms them experimentally.

Also the values of the rms's of the horizontal velocity component along the line $Y/H = 0.5$, presented in Figs. 4 and 5, panel (b), show a top-bottom asymmetry, but it is within the statistical uncertainty. The vertical component of the velocity rms along the line $Y/H = 0.5$ does not show evident asymmetries in the two cases [Fig. 4, panel (d)].

B. Turbulent kinetic energy

The turbulent kinetic energy (k) at $Z/H = 0.5$ for the NB case and the Boussinesq case is shown in Fig. 6, after scaling by $U_{\mathrm{LSC(GL)}}$ [panels (a) and (c)] and by $U_{\mathrm{LSC}(P)}$ [panels (b) and (d)]. The NB case is presented in panels (a) and (b) and the Boussinesq case in panels (c) and (d). The contour plots of both cases show similar shape and magnitude after scaling. For both cases, the regions with the highest values of k are in the vicinity of the corners. These peaks are related to the two counter-rotating rolls at the top-left and at the bottom-right corners of the cell shown in Fig. 3. The fluctuations of the velocity indeed are higher immediately before the impingement of the two vertical jet regions onto the two horizontal plates. From instantaneous flow visualizations one can see that the two vertical jet regions are unstable and oscillate before the impingement onto the horizontal walls. This leads to the high values of the turbulent kinetic energy at the top-left corner and at the bottom-right corner of the cell.

From Fig. 6, panels (a) and (b), NB effects are visible as an increase of the turbulent kinetic energy in the bottom-left quadrant of the cell with respect to the top-right quadrant. The Boussinesq reference case, plotted in panels (c) and (d) of Fig. 6 is instead more symmetric. To quantify this NB effect better, in Figs. 8 and 9 the values of the turbulent kinetic energy along the horizontal axis X/H at three different heights in the bottom-left quadrant ($Y/H = 0.1,0.2,0.3$) and in the top quadrant ($Y/H = 0.7,0.8,0.9$) are plotted for both the NB case and the Boussinesq case, with both scaling models. By comparing panels (a) and (b) of Figure. 8 (or Fig. 9), it can be seen that the values of k are slightly larger in the bottom-left quadrant of the cell shown in panel (b), with respect to the top-right quadrant shown in panel (a) for the NB case (relative increase of about 20%). In the repeated NB experiment shown in Fig. 7 and in panels (a) and (b) of Fig. 8 (and Fig. 9) as 2nd expt.; however, this NB asymmetry was not detected. The reference Boussinesq case [see panels (c) and (d) of Figs. 8 and 9] shows a good symmetry within experimental uncertainty, which was confirmed by a repeated experiment

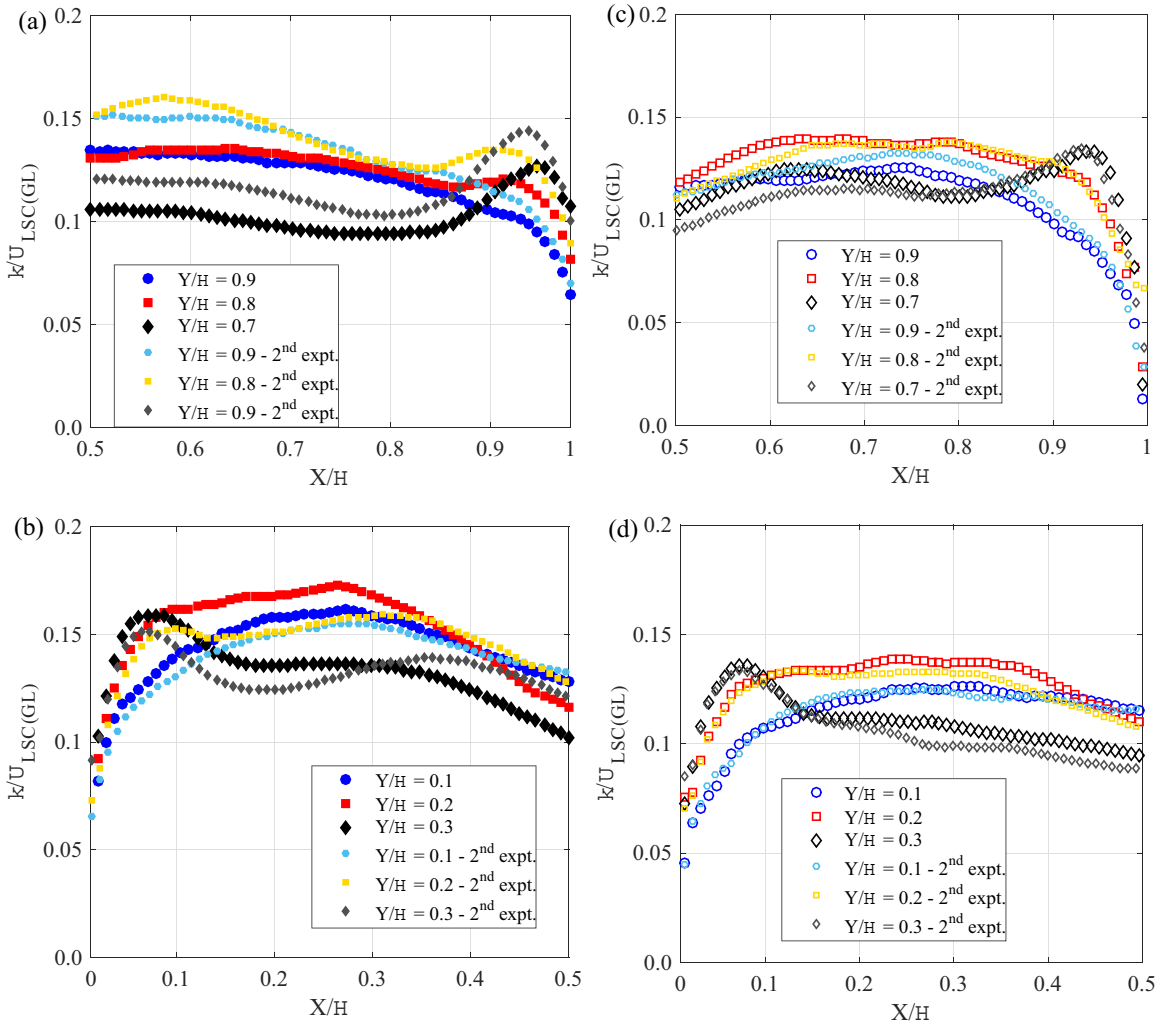

FIG. 8. One-line plots of the turbulent kinetic energy values at several heights Y/H ($Y/H = 0.1,0.2,0.3,0,7,0.8,0.9$) along the axis X/H at $Z/H = 0.5$. Values normalized by $U_{\mathrm{LSC(GL)}}$. (a), (b) Non-Boussinesq: Ra $= 6.9 \times 10^8$, Pr $= 4.33$; non-Boussinesq 2nd: Ra $= 6.84 \times 10^8$, Pr $= 4.33$. (c), (d) Boussinesq: Ra $= 6.7 \times 10^8$, Pr $= 7.24$; Boussinesq 2nd: Ra $= 6.77 \times 10^8$, Pr $= 7.24$.

shown as a contour plot in panels (c) and (d) of Fig. 7 and as one-line profiles at several heights Y/H in panels (c) and (d) of Figs. 8 and 9. The different values of k between the NB experiments may be due both to statistical uncertainty of the velocity measurements as quantified in Eqs. (6) and (7) and to a very small difference in the Rayleigh number between the two NB cases (Ra $= 6.91 \times 10^8$ in the first experiment and Ra $= 6.84 \times 10^8$ in the second).

In conclusion, from this experimental turbulent kinetic energy study it was seen that while there is symmetry at Boussinesq conditions (verified by two independent experiments), at NB conditions there is a tendency toward an asymmetric distribution of the values of k. In particular, a relative increase of the values of k was observed at the bottom-right quadrant of the cell, with respect to the top-left quadrant of about 20%. This asymmetry, however, was difficult to detect experimentally and it was not confirmed in a second experiment done at similar experimental conditions. Differences between the first and the second NB experiments were mainly due to statistical uncertainty in the velocity measurements.

V. CONCLUSIONS

Rayleigh-Bénard convection under NB conditions was investigated experimentally with particle image velocimetry in a cubical cell. The effect of the strong temperature dependency of the fluid properties on the mean velocity field and its rms values in the NB case was compared with a reference Boussinesq case done in the same setup.

To make the flow fields of the two cases dimensionless, while taking into account the influence of their different Pr numbers, the velocity values were scaled by a characteristic LSC velocity of the flow. Two LSC velocities were considered: one calculated from the Grossmann-Lohse theory [10–12] and another one calculated from the model of Pandey *et al.* [13,14]. The latter matched the experimental values of both the NB case and the Boussinesq one very well, with a relative difference of 7.5% for both cases. The U_{LSC} predicted with the GL theory instead matched the experimental values of the NB case and of the Boussinesq case with a relative difference of 73% and 60%, respectively. It was also observed that the ratio between the measured U_{LSC} for the NB case and the

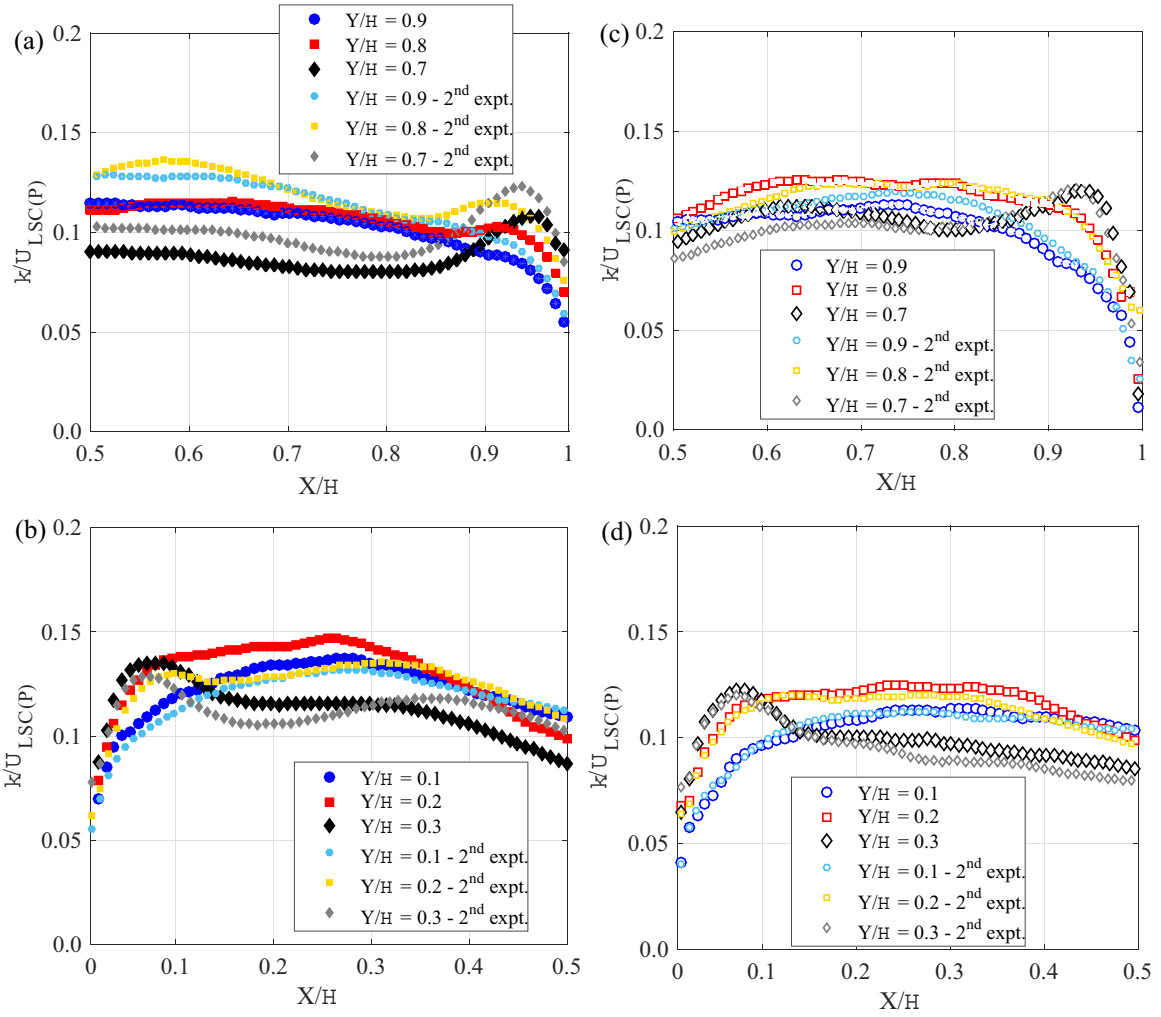

FIG. 9. One-line plots of the turbulent kinetic energy values at several heights Y/H ($Y/H = 0.1,0.2,0.3,0,7,0.8,0.9$) along the axis X/H at $Z/H = 0.5$. Values normalized by $U_{\mathrm{LSC}(P)}$. (a), (b) Non-Boussinesq: Ra $= 6.9 \times 10^8$, Pr $= 4.33$; non-Boussinesq 2nd: Ra $= 6.84 \times 10^8$, Pr $= 4.33$. (c), (d) Boussinesq: Ra $= 6.7 \times 10^8$, Pr $= 7.24$; Boussinesq 2nd: Ra $= 6.77 \times 10^8$, Pr $= 7.24$.

Boussinesq case is matched slightly better by the predictions of the GL theory, than by the Pandey model. The presented data were scaled with both LSC velocities, in order to show that the choice of one scaling velocity with respect to the other one does not make any difference with regard to the NB effect found.

A NB effect was found in the mean horizontal velocity component of the NB case, where a top-bottom asymmetry with the bottom velocity peak larger than the top one of about 13% was found. This top-bottom asymmetry of the mean velocity was seen to be very weak, just above the uncertainty limit of 7%, in the nominal Boussinesq case, where the material properties only weakly depend on temperature.

It was also seen that the value of the mean horizontal velocity component at half height of the cell is not zero for both cases, of a value that is larger than the experimental uncertainty. This shows that also the nominal Boussinesq case was influenced by the same NB effect. In the NB case, also the mean vertical velocity value at half-depth of the cell is different from zero.

Since the velocity fields of the two cases were acquired in the same setup, differences among them can be attributed to different temperature dependency of the material properties of the two fluids used in the two cases and not to the experimental setup.

This NB effect well agrees with previous numerical studies [5,6] and confirms them experimentally.

ACKNOWLEDGMENTS

This research is supported by the Dutch Technology Foundation STW, which is part of the Netherlands Organization for Scientific Research (NWO), and which is partly funded by the Ministry of Economic Affairs.

[1] Boussinesq, *Théorie analytique de la chaleur*, edited by G.-V. (Paris) (F. Didiot, Paris, 1903), Vol. 2.

[2] J. Y. Yoo, The turbulent flows of supercritical fluids with heat transfer, Annu. Rev. Fluid Mech. **45**, 495 (2013).

[3] G. Ahlers, E. Brown, F. F. Araujo, D. Funfschilling, S. Grossmann, and D. Lohse, Non-Oberbeck–Boussinesq effects in strongly turbulent Rayleigh-Bénard convection, J. Fluid Mech. **569**, 409 (2006).

[4] K. Sugiyama, E. Calzavarini, S. Grossmann, and D. Lohse, Flow organization in two-dimensional non-Oberbeck–Boussinesq Rayleigh-Bénard convection in water, J. Fluid Mech. **637**, 105 (2009).

[5] S. Horn, O. Shishkina, and C. Wagner, On non-Oberbeck–Boussinesq effects in three-dimensional Rayleigh-Bénard convection in glycerol, J. Fluid Mech. **724**, 175 (2013).

[6] S. Horn and O. Shishkina, Rotating non-Oberbeck–Boussinesq Rayleigh-Bénard convection in water, Phys. Fluids (1994-present) **26**, 055111 (2014).

[7] J. Zhang, S. Childress, and A. Libchaber, Non-Boussinesq effect: Asymmetric velocity profiles in thermal convection, Phys. Fluids (1994-present) **10**, 1534 (1998).

[8] M. Steunebrink, Effect of surface roughness on flow and heat transfer in Rayleigh-Bénard convection, Master's thesis, Delft University of Technology, The Netherlands, 2013.

[9] E. Lemmon, M. Huber, and M. McLinden, Standard Reference Data Program, 2013.

[10] S. Grossmann and D. Lohse, Scaling in thermal convection: a unifying theory, J. Fluid Mech. **407**, 27 (2000).

[11] S. Grossmann and D. Lohse, Thermal Convection for Large Prandtl Numbers, Phys. Rev. Lett. **86**, 3316 (2001).

[12] S. Grossmann and D. Lohse, Prandtl and Rayleigh number dependence of the Reynolds number in turbulent thermal convection, Phys. Rev. E **66**, 016305 (2002).

[13] A. Pandey and M. K. Verma, Scaling of large-scale quantities in Rayleigh-Bénard convection, Phys. Fluids **28**, 095105 (2016).

[14] A. Pandey, A. Kumar, A. G. Chatterjee, and M. K. Verma, Dynamics of large-scale quantities in Rayleigh-Bénard convection, Phys. Rev. E **94**, 053106 (2016).

[15] G. Ahlers, S. Grossmann, and D. Lohse, Heat transfer and large scale dynamics in turbulent Rayleigh-Bénard convection, Rev. Mod. Phys. **81**, 503 (2009).

[16] R. J. Stevens, E. P. van der Poel, S. Grossmann, and D. Lohse, The unifying theory of scaling in thermal convection: the updated prefactors, J. Fluid Mech. **730**, 295 (2013).

[17] K.-Q. Xia, C. Sun, and S.-Q. Zhou, Particle image velocimetry measurement of the velocity field in turbulent thermal convection, Phys. Rev. E **68**, 066303 (2003).

[18] K. Sugiyama, R. Ni, R. J. A. M. Stevens, T. S. Chan, S.-Q. Zhou, H.-D. Xi, C. Sun, S. Grossmann, K.-Q. Xia, and D. Lohse, Flow Reversals in Thermally Driven Turbulence, Phys. Rev. Lett. **105**, 034503 (2010).

[19] M. Chandra and M. K. Verma, Dynamics and symmetries of flow reversals in turbulent convection, Phys. Rev. E **83**, 067303 (2011).

[20] M. Chandra and M. K. Verma, Flow Reversals in Turbulent Convection via Vortex Reconnections, Phys. Rev. Lett. **110**, 114503 (2013).